The PPARβ/δ-induced mesenchymal stromal cell secretome has cytoprotective effects via ANGPTL4 in a pre-clinical model of acute lung inflammation

Courteney Tunstead[1], Molly Dunlop[1], Sinéad Ryan[1], Evelina Volkova[1], Evangeline Johnston[1], Sabrina Batah[2], Claudia C. Dos Santos[2], Bairbre McNicholas [3,4], Claire Masterson[3,4], John G. Laffey[3,4] & Karen English[1,5]

[1]*Cellular Immunology Lab, Department of Biology, Maynooth University, Maynooth, Co. Kildare, Ireland.*

[2] *Keenan Research Centre for Biomedical Research, St. Michael's Hospital, Toronto, Canada.*

[3]*Anesthesia and Intensive Care Medicine, School of Medicine, College of Medicine Nursing and Health Sciences, University of Galway, Galway, Ireland.*

[4]*Anesthesia and Intensive Care Medicine, Galway University Hospitals, Saolta University Hospitals Groups, Galway, Ireland.*

[5]*Kathleen Lonsdale Institute for Human Health Research, Maynooth University, Maynooth, Co. Kildare, Ireland.*

ABSTRACT

Rationale: Human bone marrow-derived mesenchymal stromal cells (hBM-MSCs) are known to exert immunomodulatory and pro-reparative effects *in vivo*. This makes hBM-MSCs an enticing therapeutic candidate for inflammatory diseases, such as acute respiratory distress syndrome (ARDS). The ARDS microenvironment is complex and contains an abundance of free fatty-acids (FFAs); which are known to differentially impact MSC functionality. PPARβ/**δ** is a ubiquitously expressed nuclear receptor that is activated in response to FFA-binding. It has shown to impact the therapeutic efficacy of mouse MSCs. **Objective:** This study sought to investigate the impact of PPARβ/**δ**-modulation on MSC functionality *in vitro* and *in vivo.* **Methods:** hBM-MSCs were exposed to a synthetic PPARβ/**δ** agonist/antagonist in the presence or absence of ARDS patient serum and the immunomodulatory and pro-reparative capacity of the MSC secretome was investigated using *in vitro* assays, and a pre-clinical model of LPS-induced acute lung inflammation (ALI). **Results:** Our results highlighted that the secretome from PPARβ/**δ**-agonised hBM-MSCs had enhanced pro-reparative capacity in CALU-3 lung epithelial cells by promoting the secretion of angiopoietin-like 4 (ANGPTL4). This PPARβ/**δ**-induced ANGPTL4-high MSC secretome also showed enhanced cytoprotection, wound repair, and reduced pro-inflammatory cytokines in the bronchoalveolar lavage fluid (BALF) of mice in a pre-clinical model of ALI. Importantly LPS-ALI mice that received PPARβ/**δ**-induced ANGPTL4-high MSC secretome had reduced clinical score and weight loss. This was confirmed using an anti-ANGPTL4 antibody. **Conclusion:** These findings conclude that the PPARβ/**δ**-induced ANGPTL4-high MSC secretome has anti-inflammatory, reparative and cytoprotective effects in a pre-clinical model of ALI.

INTRODUCTION

Cell therapy, particularly mesenchymal stromal cell (MSC) therapy, has long been thought of as a therapeutic candidate in the treatment of many inflammatory diseases. This is largely due to their immunomodulatory and cytoprotective capacity [1]. One of the conditions that MSCs have been considered for is acute respiratory distress syndrome (ARDS); an inflammatory, degenerative condition of the lung [2, 3]. MSCs have been trialled and tested for ARDS over the last 20 years, but clinical trials have shown poor outcomes; with ~60% non-responders [4-6]. The environment into which MSCs are administered can alter their functional capacity [7-9]. There is limited understanding of how the ARDS microenvironment may impact MSCs. The complex ARDS microenvironment contains inflammatory-mediators, microorganisms, and free fatty acids (FFAs). These components have all been shown to impact MSC therapeutic capacity in various ways [10, 11]. Our previous work highlighted the differential effect of the hypo-inflammatory vs hyper-inflammatory ARDS microenvironment on MSC therapeutic efficacy. This work showed a clear correlation between high levels of inflammation, and enhanced MSC-driven repair [12]. We, and others, have also demonstrated that FFAs can influence MSC-induced immunosuppressive effects [13, 14]. In this study, we wanted to investigate the influence of FFAs present in the ARDS patient microenvironment, and the impact they have on hBM-MSCs in a pre-clinical model of acute lung inflammation (ALI).

The peroxisome proliferator-activated receptor-beta/delta (PPARβ/**δ**) is a ubiquitously-expressed nuclear receptor, present on all nucleated cells including hBM-MSCs, that is activated in response to FFA exposure [15, 16]. In recent years, PPARβ/**δ** has been shown to impact MSC therapeutic efficacy [17-27]. Interestingly, there are differential findings with some studies showing that deficiency of PPARβ/**δ** enhances MSC immunosuppressive effects [21, 22], while other studies demonstrate similar immunosuppressive effects mediated by both

naive and PPARβ/**δ**-deficient mouse MSCs [24]. Studies have shown enhanced immunomodulatory capacity of T-cells by PPARβ/**δ**-inhibited mouse MSCs [21, 22]. Differentialy, PPARβ/**δ** antagonism of MSCs impaired MSC therapeutic effects while priming of mouse MSCs with a PPARβ/**δ** agonist enhanced MSC cardioprotective effects *in vivo* [25]. Moreover, cardioprotective effects of MSCs were shown to be PPARβ/**δ**-dependent as the therapeutic effect was lost when PPARβ/**δ**-deficient mouse MSCs were administered [24]. These findings suggest that natural ligands of PPARβ/**δ** may have positive or detrimental effects on MSC efficacy *in vivo*. Due to the abundance of FFAs in the ARDS microenvironment, we sought to investigate the impact of PPARβ/**δ** (via synthetic agonism or antagonism) on the human BM-MSC secretome; and report the impact this had on immunomodulation and cytoprotection, in a model of ALI.

MATERIALS AND METHODS

hBM-MSC cell culture

Human bone marrow-derived MSCs (hBM-MSCs; RoosterBio™) were cultured in Dulbecco's Modified Eagle Medium (DMEM) containing 10% Foetal Bovine Serum (FBS) and 1% *Penicillin streptomycin* (cDMEM). The cells were cultured for 5 days at 37°C + 5% CO_2. All experiments are a representation of three independent MSC donors.

Generation and concentration of MSC-CM

hBM-MSCs (passage 2-5) from three independent donors were seeded at a density of $1x10^5$ per well in a 6-well plate in 1ml of cDMEM and left to attach. Once attached, the cells were stimulated with 1µM of PPARβ/**δ** agonist (GW0742, Tocris™) or antagonist (GSK3787, Tocris™), as previously done in our group [12]. 24hr-post stimulation, the cells were washed with PBS, and the media was replaced with serum-free DMEM. This was left for a further 24hrs to allow for the generation of MSC-CM. When including ARDS serum-exposure, the agonist/antagonist were washed from the cells, and 20% ARDS serum was added for 24hrs. This was then washed away, and serum-free DMEM was added for a further 24hrs to allow for the generation of MSC-CM. All MSC-CM was harvested and stored at -20°C for future experiments. MSC-CM was then concentrated, as required, as previously described [12].

Gene & Protein expression

For gene expression, RNA was isolated and normalised to 100 ng/µl. cDNA was made using the QuantBio™ cDNA Synthesis kit (as per manufacturer's instructions). Real-time Polymerase Chain Reaction (RT-PCR) was run using PerfeCta SYBR Green FastMix (QuantBio™) and pre-made Sigma™ primers (supplementary table 1). Relative expression

was quantified in relation to *hprt* by calculating the 2-ΔΔCT values. For protein expression, 96-well half-area ELISA plates (COSTAR™) were coated as per manufacturers guidelines (human ANGPTL4 and VEGF (R&D™)) and run as previously described [12].

Sequencing & metabolomic analysis

hBM-MSCs were seeded at a density of $1x10^5$ in a 6-well plate and left to adhere. Once attached, the cells were exposed to 1μM of PPARβ/**δ** agonist (GW0742, Tocris™) or antagonist (GSK3787, Tocris™) and left for 6hrs. This dose was chosen based on previous research from our group [19]. The cells were harvested in TRIzol for RNA isolation. RNA was isolated through a series of chloroform and isopropanol extractions. RNA concentration and purity was assessed using Nanodrop 2000 (Thermofisher) and samples were sent to Novogene™ for sequencing (GEO accession no.: GSE281162). Processed RNA sequencing datasets, provided by Novogene™, were then used to identify differentially expressed genes (DEGs) of interest. Volcano plots, highlighting the most significantly enriched genes, were generated using Flourish™ software. Data was also collected from publicly available RNA sequencing (GEO accession no.: GSE185263) and metabolomic datasets (Study ID: ST000042; doi: 10.21228/M8SG64). Normalised values were taken from both studies and data was plotted using GraphPad Prism™ (version 10) software.

Scratch Assay

CALU-3 lung epithelial cells (cultured as previously described) [12] were seeded at a density of $5x10^5$ in a 6-well plate. Once 80% confluent, a single vertical scratch was made down the centre of the well using a p200 tip. The cells were then washed with PBS to remove debris, and MSC-CM was added for a period of 6-48hrs. The cells were then fixed with 10% formalin, before leaving to dry. Once dry, the cells were stained with crystal violet, left to dry, and

imaged. To avoid bias, a marker was used to denote an area in the upper, central and lower regions of each scratch and images were taken from these points (supplementary figure 1). Mitomycin C (Sigma™) was added to assess the impact of proliferation at a concentration of 5 µg/ml for 2hrs prior to the scratch assay.

Scratch Assay Analysis

Three images, taken at each of the three marked points, were taken per well; for each of the three independent MSC donors (i.e. 3 images per well x 3 MSC donors = 9 images per group). Fiji/ImageJ™ software was then used to divide each picture into four distinct quadrants in an unbiased manner (Analyse -> Tools -> Grid -> set area per point to 44444 inches squared). This grid includes the addition of 4 horizontal lines imputed on the image. Using the straight-line feature in Fiji/ImageJ™ software, four measurements were then taken per picture at each of the horizontal lines. This provided 4 measurements per picture, at unbiased points, to get a clear depiction of each percentage wound closure. The average wound closure per donor was calculated, and divided by the baseline scratch value, to get the final percentage wound closure (supplementary figure 1).

Study cohorts and ethical approval for patient samples

Ethical approval was obtained from Galway University Medical Ethics Committee and Maynooth University Ethics Committee. All participants provided full consent.

ARDS serum extraction

Serum samples from both male and female patients, aged 40-80 years old, were taken from patients with SARS-CoV-2-induced ARDS, from the patient pools we previously characterised and described [12].

ANGPTL4 Neutralisation

MSC-CM was exposed to 5 µg/ml of ANGPTL4 neutralising antibody (Cell Sciences™), or 5 µg/ml IgG2aκ isotype control (Rockland Immunochemicals™). This was incubated at room temperature for 1hr prior to use. This concentration was utilised as per manufacturer guidelines for our study.

ALI mouse model

Male and female C57BL6/J mice (Charles River), aged 8+ weeks, 2mg/kg of endotoxin (Sigma, 0001:B4 Serotype), or PBS control, was administered intratracheally (IT) and observed twice daily for 48hrs. MSC-CM was prepared as described above. 500µl of PPARβ/**δ**-modulated MSC-CM, i.e. the equivalent of what would be produced from $5x10^4$ (low dose) of hBM-MSCs, was then concentrated to a volume of 30µl and administered intranasally (IN) 4hrs post-endotoxin challenge per mouse. An Evan's Blue permeability assay was carried out by administration of an intravenous (IV) tail vein injection of sterile-filtered Evan's Blue Dye (10%) 1hr prior to harvesting. The mice were sacrificed using an intraperitoneal (IP) injection of pentobarbital. Absorbance readings were taken to assess the total Evan's blue (620nm and 740nm) in BALF, blood and whole lungs.

Statistical analysis of animal studies

Power calculations were performed to guide sample size and data was analysed using GraphPad Prism™ (version 10) software. Statistical tests used have been highlighted in the figure legends of each figure.

RESULTS

The $MSC_{PPARβ/δ(+)}$ secretome enhances pro-reparative capacity in CALU-3 lung epithelial cells via migration and proliferation *in vitro*

A scratch assay in CALU-3 cells was used to investigate the impact of PPARβ/**δ** agonism (+) or antagonism (-) on MSC conditioned medium (MSC-CM) capacity to promote wound healing *in vitro* (figure 1A). Our data highlighted a significant increase in wound closure in both MSC-CM_{Naive} and MSC-$CM_{PPARβ/δ(+)}$ groups (figure 1B, C). It is known that wound closure can involve proliferation and or migration [28, 29], thus this experiment was repeated using Mitomycin C; a known proliferation inhibitor [30]. While the addition of Mitomycin C significantly reduced wound closure in the MSC-CM_{Naive} and MSC-$CM_{PPARβ/δ(+)}$ groups at the 48hr time point, the percentage wound healing in these groups with Mitomycin C remained higher than the DMEM only group suggesting that both proliferation and migration had a combination effect (figure 1D). Interestingly, significantly more wound repair was observed in our MSC-$CM_{PPARβ/δ(+)}$ group compared to our MSC-CM_{Naive} group, while the MSC-$CM_{PPARβ/δ(-)}$ group did not inhibit or enhance would healing (figure 1D). *TOP2A is* a gene largely indicative of cell proliferation [31] and has previously been used as an indicator for cell proliferation in wound healing. Gene expression analysis of *TOP2A* in CALU-3 cells highlighted a significant difference between the MSC-$CM_{PPARβ/δ(+)}$ and MSC-$CM_{PPARβ/δ(-)}$ groups, with the MSC-$CM_{PPARβ/δ(+)}$ group having significantly more proliferative capacity than the MSC-$CM_{PPARβ/δ(+)}$ group (figure 1E).

Analysis of $MSC_{PPARβ/δ(+)}$ RNA sequencing highlighted upregulation of several genes

To try to identify the potential mechanisms associated with enhanced wound healing capacity in $MSC_{PPARβ/δ(+)}$, RNA sequencing (Novogene™; GEO accession no.: GSE281162) was

performed on $MSC_{PPARβ/δ(+)}$, $MSC_{PPARβ/δ(-)}$ and MSC_{Naive} (figure 2A). The data highlighted a variety of differentially expressed genes (DEGs) between the three groups. The DEGs were visualised using a Venn diagram (figure 2B), showing 170 DEGs specific to the MSC_{Naive} group, 128 specific to the $MSC_{PPARβ/δ(+)}$ group, and 189 specific to the $MSC_{PPARβ/δ(-)}$ group. Volcano plot visualisation highlighted several of the most significantly altered DEGs in each group (figure 2C). The $MSC_{PPARβ/δ(+)}$ group had a significant enrichment of genes such as *PLIN2, ANGPTL4, FAM156A, CPT1A, CAT, NADK2, TMED6,* and *LDHAL6B.* This group also showed significant downregulation in genes such as *MAGED4* and *FAM157B* (table 1). The $MSC_{PPARβ/δ(-)}$ group had a significant enrichment of genes such as *IKBKGP1, SNRPGP2, LINC01159, MIR3648-1, RARRES1, MALAT1* and *RNF217-AS1.* This group also showed significant downregulation in genes such as *RGPD5, PFN1P3, MIR3936HG, U2AF1* and *TSNAXIP1*(table 2). Fragments per kilobase of exon per million mapped fragments (FPKMs) of two known PPARβ/**δ** target genes were plotted to confirm the data was as expected (figure 2D, E), and this was confirmed by qRT-PCR (figure 2F, G).

MSC-associated genes/proteins are unaffected by PPARβ/δ agonism or antagonism; except ANGPTL4

Given the functional enhancement of $MSC\text{-}CM_{PPARβ/δ(+)}$ promotion of wound healing observed in figure 1, the production of known cytoprotective factors released by MSCs were assessed. While MSC_{Naive} produced ANGPTL4, VEGF and MIF, $MSC_{PPARβ/δ(+)}$ only produced significantly higher levels of ANGPTL4 (figure 3A-C). This aligns with the RNA-sequencing data as *ANGPTL4* was the only cytoprotective factor differentially expressed in $MSC_{PPARβ/δ(+)}$. Along with this, PPARβ/**δ** agonism/antagonism did not affect expression of typical MSC-associated immunomodulatory factors such as *PTGS2, IL-6, IDO, PTGES* or *TGFβ (figure 3D-H).*

The MSC-CM$_{PPARβ/δ(+)}$ enhances wound healing in CALU-3 lung epithelial cells in an ANGPTL4-dependent manner

Other studies have highlighted the role of a PPARβ/**δ** agonist in repair [18], and the impact ANGPTL4 can have on repair in other tissues [29, 32]. It has also already been shown that ANGPTL4 can play a significant role in proliferation and migration [28]. To determine if the increased levels of ANGPTL4 present in MSC-CM$_{PPARβ/δ(+)}$ was the true mechanism behind the enhanced pro-reparative capacity, we made use of an anti-ANGPTL4 neutralising-antibody to eliminate the functional capacity of ANGPTL4 in the MSC-CM (figure 4A). This would prevent it from acting on the CALU-3 lung epithelial cells. Scratch assay analysis from each of our groups, whereby the MSC-CM used was exposed to either the ANGPTL4 neutralising antibody or a corresponding IgG control, highlighted that ANGPTL4-neutralisation abrogated the enhanced wound closure once seen in the MSC-CM$_{PPARβ/δ(+)}$ group (figure 4B-C). The ability of the ANGPTL4 neutralising antibody to interfere with ANGPTL4 was quantified by ELISA (figure 4D).

Ligands and co-activators of PPARβ/δ are increased, while co-repressors of PPARβ/δ are decreased, in ARDS patients

Thus far, PPARβ/**δ** agonism has shown to enhance the cytoprotective effects of MSC-CM. Previously, it was deduced that MSC-CM derived from ARDS-serum licensed MSCs has superior therapeutic effects in a pre-clinical model of ALI [12]. To ensure translational relevance of our findings from this study in human conditions such as ARDS, a publicly available metabolomics dataset (Study ID: ST000042; doi: 10.21228/M8SG64) was mined and it was identified that PPARβ/**δ** ligands are more prevalent in ARDS. Higher levels of linoleate, palmitoleic acid and arachidonate were present in the bronchoalveolar lavage fluid (BALF)

from ARDS patients, in comparison to healthy controls (figure 5A). Using a publicly available RNA sequencing dataset (GEO accession no.: GSE185263), it was shown that several PPARβ/**δ**-associated co-activators that were increased in the blood of ARDS patients (figure 5B). This included a significant increase in *NCOA1* and *NCOA3,* a trend toward increased *PPARGC1A* and *NCOA2,* and no difference in *CREBBP* (figure 5C-G). Along with this, several PPARβ/**δ**-associated co-repressors were decreased in the blood of the same ARDS patients (figure 5B). This included a significant reduction in *SIRT1, NCOR1* and *NCOR2* (figure 5H-J). Given that *ANGPTL4* was significantly upregulated in the sequencing dataset, this was further assessed upon MSC-exposure to ARDS patient serum. In comparison to the PPARβ/**δ** agonist, exposure of MSCs to ARDS patient serum significantly increased MSC secretion of ANGPTL4. Addition of both the PPARβ/**δ** agonist and ARDS patient serum further enhanced MSC production of ANGPTL4 (figure 5K). Interestingly, addition of the PPARβ/**δ** antagonist could not block the ARDS serum induction of ANGPTL4 secretion by MSCs. This is largely down to PPARβ/**δ** having multiple binding-sites [33], whereby both agonists and antagonists can bind simultaneously; with agonism always out-competing antagonism (supplementary figure 2).

ARDS-licensed MSC-CM$_{PPARβ/δ(+)}$ provides enhanced therapeutic effects in ALI in an ANGPTL4 dependent manner

Next, investigation into the protective effects of MSC-CM$_{PPARβ/δ(+)}$ were assessed in a preclinical model of LPS induced-ALI. In a pilot study, a low dose of MSCs (5 x 10^4) with reduced therapeutic efficacy was determined in ALI, alongside a higher dose of MSCs (1x10^5) demonstrating efficacy (supplementary figure 3). Following this, MSC-CM that was generated from the equivalent of the low dose was used; with the idea that we would detect enhanced therapeutic efficacy following PPARβ/**δ** agonism or antagonism. This showed that MSC-

$CM_{PPARβ/δ(+)}$ but not MSC-$CM_{PPARβ/δ(-)}$ significantly improved the therapeutic efficacy of the non-efficacious dose of MSC-CM; by enhancing vascular and epithelial barrier function as measured using Evans blue dye assay (figure 6A, B). Although modest, this result was statistically powered. This effect was somewhat impacted by pre-exposing the MSC-CM to anti-ANGPTL4 neutralising antibody, but this was not significantly different from the MSC-$CM_{PPARβ/δ(+)}$ group (figure 6A, B). MSC-$CM_{PPARβ/δ(+)}$ also significantly reduced the level of TNFα in the BALF of LPS-exposed mice (figure 6C). However, ANGPTL4-neutralisation could not reverse this effect (figure 6C). MSC-$CM_{PPARβ/δ(+)}$ had no effect on IL-6 (figure 6D) or total protein (figure 6E) in the BALF. Interestingly exposure to ARDS patient serum, along with PPARβ/**δ** agonism, allowed for a 10-fold increased induction of ANGPTL4 in MSC-CM compared to PPARβ/**δ** agonist alone (figure 5K). Other proteins examined including IL-6, IL-8, VEGF, IL-1β and MIF (supplementary figure 4) were not increased in MSCs that had been exposed to ARDS patient serum, along with PPARβ/**δ** agonism. Next, investigation into the efficacy of ARDS-licensed MSC-$CM_{PPARβ/δ(+)}$ in the ALI model. In this case, the combination of ARDS serum and PPARβ/**δ** agonism led to significantly enhanced therapeutic effects with significant reduction in TNFα and IL-6 in the BALF (figure 6C, D). Importantly, anti-ANGPTL4 reduced the anti-inflammatory effects mediated by the ARDS-licensed MSC-$CM_{PPARβ/δ(+)}$. Although there was no significant reduction in total protein, the trend toward a reduction in total protein was abrogated in the presence of the anti-ANGPTL4 neutralising antibody (figure 6E).

ARDS-licensed MSC-$CM_{PPARβ/δ(+)}$ reduced the severity of the clinical score and percentage weight-loss in ALI in an ANGPTL4 dependent manner

Following on from our pre-clinical study, the clinical scores and percentage weight-loss were plotted (figure 6F, G). Interestingly, we saw a non-significant trend toward a reduced clinical

score in mice exposed to ARDS-licensed MSC-CM$_{PPARβ/δ(+)}$ (figure 6F) and this was not seen in the non-licensed group. ANGPTL4-neutralisation abrogated this effect (figure 6F). Along with this, percentage weight-loss was also observed. There was a significant reduction in percentage weight-loss in mice exposed to ARDS-licensed MSC-CM$_{PPARβ/δ(+)}$ (figure 6G), and again, this effect was abrogated in the presence of the anti-ANGPTL4-neutralising antibody (figure 6G).

DISCUSSION

There are two primary functions of MSCs in the context of cell therapy: immunomodulation and pro-repair [1]. It is known that the environment can largely dictate MSC response [7, 11, 34]. In the context of ARDS, the complex patient microenvironment; containing inflammatory-agents, microorganisms and FFAs, can notably impact MSC functionality [10, 35]. We previously highlighted that higher levels of inflammation in the ARDS patient microenvironment can promote VEGF-driven repair [12]. Abreu *et al.* (2020) investigated the detrimental impact of fungal toxins present in the lung on MSC viability and showed a drastic increase in MSC cell-death in response to this microenvironmental element [7]. However, there has been little focus on how the FFAs in the ARDS patient microenvironment may impact MSCs [36]. FFAs are known natural ligands of PPARβ/**δ** [37-39]. Importantly, studies have already shown that modulation of this receptor can alter MSC functionality [17, 20, 21, 23, 25]. Given this, we wanted to investigate the functional impact of PPARβ/**δ**-modulation on both primary functions of MSCs; immunomodulation and/or pro-reparative capacity.

In the case of pro-reparative capacity, PPARβ/**δ**-activation enhanced MSC-CM mediated wound repair in CALU-3 lung epithelial cells (figure 1B, C). A time-lapse

experiment, using a mitomycin C proliferation inhibitor, highlighted that this was likely a combination effect of both migration and proliferation (figure 1D, E). In the context of promoting tissue repair, MSC secretion of VEGF [40-43], and HGF [44, 45] among other factors have been shown to play key roles. However, PPARβ/**δ**-activation did not lead to differential expression of VEGF or HGF. Interestingly, ANGPTL4 was significantly increased in PPARβ/**δ** agonised MSCs. It has already been shown in several studies that ANGPTL4 can promote both migration and proliferation in endothelial cells [28, 29]. Ziveri *et al.* (2024) recently published a comprehensive study on the role of ANGPTL4 in endothelial cytoprotection in skin vs brain endothelial cells. They identified that ANGPTL4 in the brain endothelium protects against bacterial sepsis, and upon addition of ANGPTL4 to the skin endothelium (which naturally has lower levels of ANGPTL4), they demonstrated protection against bacterial sepsis [27]. Moreover, ANGPTL4 has been shown to improve cardiac function in a mouse model of myocardial infarction [46]. Human MSCs produced increased levels of ANGPTL4 following co-culture with THP-1 macrophages *in vitro* [46]. Based on the identification of increased expression of ANGPTL4 in PPARβ/**δ** agonised MSCs in our RNA-seq data set, we used an anti-ANGPTL4 antibody to neutralise the ANGPTL4 in the MSC secretome, before addition to the CALU-3 lung epithelial cells (figure 4B-D). This abrogated the enhanced wound closure we had originally observed in our MSC-$CM_{PPARβ/δ(+)}$ group.

We identified increased levels of PPARβ/**δ** ligands and co-activators in ARDS patient samples using publicly available datasets. Exposure of MSCs to ARDS patient serum samples significantly increased ANGPTL4 levels. A combination of MSC exposure to ARDS patient serum and a PPARβ/**δ** agonist further increased ANGPTL4 levels. This proves that MSCs are receptive to FFAs/other PPARβ/**δ** ligands presents in the ARDS microenvironment. This aligns to our previous study where we identified that human BM-MSCs produce significantly increased levels of ANGPTL4 in response to the FFA palmitate [14].

To enhance the clinical relevance of our findings, we showed that MSC-CM$_{PPARβ/δ(+)}$ mediated protective effects in ALI significantly enhancing vascular and epithelial barrier integrity *in vivo*. Indeed, other studies have demonstrated that MSC-CM can mediate therapeutic effects *in vivo* in ALI models [47] including our own study [12]. Using MSC-CM generated from the equivalent of half the dose of MSC-CM used in our previous study [12]. This allowed us to observe whether MSC-CM$_{PPARβ/δ(+)}$ provided enhanced efficacy over and above MSC-CM$_{PPARβ/δ(-)}$ in a pre-clinical model of ALI. While there was a significant difference in the capacity for MSC-CM$_{PPARβ/δ(+)}$ in enhancing barrier function, addition of the ANGPTL4-neutralising antibody failed to significantly impair this effect. Our study demonstrated that ARDS patient serum induced significantly higher levels of ANGPTL4 in MSC-CM and that combination with a PPARβ/**δ** agonist further increased it. While MSC-CM$_{PPARβ/δ(+)}$ did not significantly reduce proinflammatory cytokines in the BALF, ARDS licensed MSC-CM$_{PPARβ/δ(+)}$ significantly reduced TNFα in the BALF of ALI mice. By combining the PPARβ/**δ** agonist and licensing with ARDS patient serum, we created MSC-CM with greater immunosuppressive capacity when compared to MSC-CM$_{PPARβ/δ(+)}$ alone. This is likely associated with the ~10-fold increase in ANGPTL4 levels when using the combined licensing approach as addition of the ANGPTL4 neutralising antibody reversed the trend.

Here we provide novel findings to demonstrate that human BM-MSCs are responsive to FFAs present in the ARDS patient environment, leading to significantly increased levels of ANGPTL4 production. For the first time, we show that MSC-derived ANGPTL4 plays an important role in promoting epithelial repair and enhancing vascular barrier integrity. As most published studies have focused on mouse MSCs, we have also addressed the gap in the knowledge of how PPARβ/**δ** influences human BM-MSC cytoprotective and immunosuppressive functions. In this study, focusing on ALI, we did not detect any positive

or negative effects associated with PPARβ/**δ** antagonism in hBM-MSCs. However, PPARβ/**δ** agonism enhanced MSC-CM promotion of wound healing *in vitro* and vascular and barrier integrity *in vivo*. Furthermore, the combined approach of PPARβ/**δ** agonism and licensing with ARDS patient serum produced an MSC-CM that could suppress pro-inflammatory cytokines in the BALF of ALI mice.

Author Contributions

C.T. performed research, data analysis, and study design and wrote the manuscript. M.D., S.R., E.V., E.J., S.B. and C.M. provided expertise and or performed research and data analysis. B.McN and J.G.L. provided patient samples and data for the study. C.C.D.S and J.G.L. contributed to study design. K.E. designed and supervised the study and wrote the manuscript. All authors approved the final manuscript.

Funding

This research was supported by a Science Foundation Ireland Award to K.E. and J.G.L (20/FFP-A/8948). This publication has emanated from research supported in part by the National Irish Covid Biobank, through which our patient samples were collected and stored.

Competing interests

The authors declare no conflicts of interest.

Ethical Approval and HPRA Compliance

Ethical approval was granted by the Maynooth University research ethics committee (BRESC-2022-2453953) under the title: Cell based therapeutics for acute respiratory distress syndrome for the animal studies and by Galway University Hospitals Research Ethics Committee and by

the Maynooth University research ethics committee (BSRESC-2022-2482563) under the title: Human serum Sepsis/ARDS MSC. HPRA approval was granted under the project authorisation(s) AE19124/P031/P037.

Data availability statement

The RNA-sequencing dataset generated in our lab is available through GEO accession no.: GSE281162. The other publicly available data sets are available online as outlined in the Methods section. The remaining data supporting the findings of this study are available upon request from the corresponding author.

Acknowledgements

The authors are grateful to the ARDS patients who donated the samples used in this study. We would like to thank Deirdre Daly and Gillian O'Meara for the outstanding care of the animals used in this study. Schematic figures contained in this manuscript have been created using biorender.com.

Table 1: DEG functions in $MSC_{PPARβ/δ(+)}$ group.

Gene name	Up/Down	Involved in
plin2	Up	Lipid metabolism
angptl4	Up	Lipid metabolism and angiogenesis
fam156A	Up	Enables protein binding
cpt1A	Up	Lipid metabolism
cat	Up	Protection against oxidative stress

nadk2	Up	Protection against oxidative stress
tmed6	Up	Trafficking and transport
ldhal6B	Up	Lactate metabolism
maged4	Down	Cell cycle regulation
fam157B	Down	Non-coding

Table 2: DEG functions in $MSC_{PPARβ/δ(-)}$ group.

Gene name	**Up/Down**	**Involved in**
ikbkgp1	Up	NFκB signalling
snrpgp2	Up	RNA processing
linc01159	Up	Cell differentiation
mir3648-1	Up	Cell differentiation
rarres1	Up	Cell differentiation & retinoid signalling
malat1	Up	Cell differentiation
rnf217-as1	Up	Cell differentiation
rgpd5	Down	GTPase regulation
pfn1p3	Down	Cell motility/migration
mir3936hg	Down	Proliferation and apoptosis
u2af1	Down	ROS production/oxidative stress
tsnaxip1	Down	RNA processing and transport

REFERENCES

1. Faircloth, T.U., et al., *Vascular endothelial growth factor secretion and immunosuppression are distinct potency mechanisms of human bone marrow mesenchymal stromal cells.* Stem Cells, 2024. **42**(8): p. 736-751.
2. Matthay, M.A. and G.A. Zimmerman, *Acute lung injury and the acute respiratory distress syndrome: four decades of inquiry into pathogenesis and rational management.* Am J Respir Cell Mol Biol, 2005. **33**(4): p. 319-27.
3. Yang, X., et al., *Clinical course and outcomes of critically ill patients with SARS-CoV-2 pneumonia in Wuhan, China: a single-centered, retrospective, observational study.* Lancet Respir Med, 2020. **8**(5): p. 475-481.
4. Kaffash Farkhad, N., et al., *Mesenchymal stromal cell therapy for COVID-19-induced ARDS patients: a successful phase 1, control-placebo group, clinical trial.* Stem Cell Res Ther, 2022. **13**(1): p. 283.
5. Bowdish, M.E., et al., *A Randomized Trial of Mesenchymal Stromal Cells for Moderate to Severe Acute Respiratory Distress Syndrome from COVID-19.* Am J Respir Crit Care Med, 2023. **207**(3): p. 261-270.
6. Gorman, E., et al., *Repair of acute respiratory distress syndrome by stromal cell administration (REALIST) trial: A phase 1 trial.* EClinicalMedicine, 2021. **41**: p. 101167.
7. Abreu, S.C., et al., *Differential effects of the cystic fibrosis lung inflammatory environment on mesenchymal stromal cells.* Am J Physiol Lung Cell Mol Physiol, 2020. **319**(6): p. L908-L925.
8. Hawthorne, I.J., et al., *Human macrophage migration inhibitory factor potentiates mesenchymal stromal cell efficacy in a clinically relevant model of allergic asthma.* Mol Ther, 2023. **31**(11): p. 3243-3258.

9. Corbett, J.M., et al., *Cyclosporine A and IFNγ licencing enhances human mesenchymal stromal cell potency in a humanised mouse model of acute graft versus host disease.* Stem Cell Res Ther, 2021. **12**(1): p. 238.

10. Dunbar, H., et al., *The Inflammatory Lung Microenvironment; a Key Mediator in MSC Licensing.* Cells, 2021. **10**(11).

11. Rolandsson Enes, S., et al., *Healthy versus inflamed lung environments differentially affect mesenchymal stromal cells,* Eur Respir J, 2021. **58**(4).

12. Tunstead, C., et al., *The ARDS microenvironment enhances MSC-induced repair via VEGF in experimental acute lung inflammation.* Mol Ther, 2024. **32**(10): p. 3422-3432.

13. Boland, L., et al., *IFN-γ and TNF-α Pre-licensing Protects Mesenchymal Stromal Cells from the Pro-inflammatory Effects of Palmitate.* Mol Ther, 2018. **26**(3): p. 860-873.

14. Tunstead, C., Bitterlich, L.B.*, Ankrum, J.A., Hogand, A.E. and English, K., *Palmitate enhances MSC immunomodulation of human macrophages via the ceramide/CCL2 axis in vitro.* Stem Cell Research and Therapy, 2025.

15. Liu, Y., et al., *The Role of PPAR-δ in Metabolism, Inflammation, and Cancer: Many Characters of a Critical Transcription Factor.* Int J Mol Sci, 2018. **19**(11).

16. Kota, B.P., T.H. Huang, and B.D. Roufogalis, *An overview on biological mechanisms of PPARs.* Pharmacol Res, 2005. **51**(2): p. 85-94.

17. Lim, J. and E.K. Park, *Effect of fibroblast growth factor-2 and retinoic acid on lineage commitment of bone marrow mesenchymal stem cells.* Tissue Eng Regen Med, 2016. **13**(1): p. 47-56.

18. Park, J.R., et al., *Effects of Peroxisome Proliferator-Activated Receptor-δ Agonist on Cardiac Healing after Myocardial Infarction.* PLoS One, 2016. **11**(2): p. e0148510.

19. Carty, F., et al., *IFN-γ and PPARδ influence the efficacy and retention of multipotent adult progenitor cells in graft vs host disease.* Stem Cells Transl Med, 2021. **10**(11): p. 1561-1574.

20. Heck, B.E., et al., *PPAR-δ Agonist With Mesenchymal Stem Cells Induces Type II Collagen-Producing Chondrocytes in Human Arthritic Synovial Fluid.* Cell Transplant, 2017. **26**(8): p. 1405-1417.

21. Luz-Crawford, P., et al., *PPARβ/δ directs the therapeutic potential of mesenchymal stem cells in arthritis.* Ann Rheum Dis, 2016. **75**(12): p. 2166-2174.

22. Contreras-Lopez, R.A., Elizondo-Vega, R., Torres, M.J. *et al*, *PPARβ/δ-dependent MSC metabolism determines their immunoregulatory properties.* 2020: p. 11423

23. Kim, D.H., et al., *PPAR-δ agonist affects adipo-chondrogenic differentiation of human mesenchymal stem cells through the expression of PPAR-γ.* Regen Ther, 2020. **15**: p. 103-111.

24. Nernpermpisooth, N., et al., *PPARβ/δ Is Required for Mesenchymal Stem Cell Cardioprotective Effects Independently of Their Anti-inflammatory Properties in Myocardial Ischemia-Reperfusion Injury.* Front Cardiovasc Med, 2021. **8**: p. 681002.

25. Sarre, C., et al., *PPARβ/δ priming enhances the anti-apoptotic and therapeutic properties of mesenchymal stromal cells in myocardial ischemia-reperfusion injury.* Stem Cell Res Ther, 2022. **13**(1): p. 167.

26. Djouad, F., et al., *PPARβ/δ: A master regulator of mesenchymal stem cell functions.* Biochimie, 2017. **136**: p. 55-58.

27. Ziveri, J., et al., *Angiopoietin-like 4 protects against endothelial dysfunction during bacterial sepsis.* Nat Microbiol, 2024. **9**(9): p. 2434-2447.

28. Goh, Y.Y., et al., *Angiopoietin-like 4 interacts with integrins beta1 and beta5 to modulate keratinocyte migration.* Am J Pathol, 2010. **177**(6): p. 2791-803.

29. Zhan, W., et al., *ANGPTL4 attenuates palmitic acid-induced endothelial cell injury by increasing autophagy.* Cell Signal, 2022. **98**: p. 110410.

30. An, Q., et al., *In vitro effects of mitomycin C on the proliferation of the non-small-cell lung cancer line A549.* Int J Clin Exp Med, 2015. **8**(11): p. 20516-23.

31. Neubauer, E., et al., *Comparative evaluation of three proliferation markers, Ki-67, TOP2A, and RacGAP1, in bronchopulmonary neuroendocrine neoplasms: Issues and prospects.* Oncotarget, 2016. **7**(27): p. 41959-41973.

32. Huang, W., et al., *ANGPTL4 induces Kupffer cell M2 polarization to mitigate acute rejection in liver transplantation.* Sci Rep, 2025. **15**(1): p. 986.

33. Batista, F.A., et al., *Structural insights into human peroxisome proliferator activated receptor delta (PPAR-delta) selective ligand binding.* PLoS One, 2012. **7**(5): p. e33643.

34. Kornicka, K., J. Houston, and K. Marycz, *Dysfunction of Mesenchymal Stem Cells Isolated from Metabolic Syndrome and Type 2 Diabetic Patients as Result of Oxidative Stress and Autophagy may Limit Their Potential Therapeutic Use.* Stem Cell Rev Rep, 2018. **14**(3): p. 337-345.

35. Lu, P., et al., *Serum Free Fatty Acid Concentration Predicts ARDS after Off-Pump CABG: A Prospective Observational Study.* Lung, 2024. **202**(5): p. 523-532.

36. Boland, L., et al., *Translating MSC Therapy in the Age of Obesity.* Front Immunol, 2022. **13**: p. 943333.

37. Grygiel-Górniak, B., *Peroxisome proliferator-activated receptors and their ligands: nutritional and clinical implications--a review.* Nutr J, 2014. **13**: p. 17.

38. Mirza, A.Z., I.I. Althagafi, and H. Shamshad, *Role of PPAR receptor in different diseases and their ligands: Physiological importance and clinical implications.* Eur J Med Chem, 2019. **166**: p. 502-513.

39. Capelli, D., et al., *Structural basis for PPAR partial or full activation revealed by a novel ligand binding mode.* Sci Rep, 2016. **6**: p. 34792.

40. Yang, Y., et al., *Synergism of MSC-secreted HGF and VEGF in stabilising endothelial barrier function upon lipopolysaccharide stimulation via the Rac1 pathway.* Stem Cell Res Ther, 2015. **6**: p. 250.

41. Zisa, D., et al., *Vascular endothelial growth factor (VEGF) as a key therapeutic trophic factor in bone marrow mesenchymal stem cell-mediated cardiac repair.* Biochem Biophys Res Commun, 2009. **390**(3): p. 834-8.

42. Yang, Y., et al., *The Vascular Endothelial Growth Factors-Expressing Character of Mesenchymal Stem Cells Plays a Positive Role in Treatment of Acute Lung Injury In Vivo.* Mediators Inflamm, 2016. **2016**: p. 2347938.

43. Dunbar, H., et al., *The VEGF-Mediated Cytoprotective Ability of MIF-Licensed Mesenchymal Stromal Cells in House Dust Mite-Induced Epithelial Damage.* Eur J Immunol, 2025. **55**(1): p. e202451205.

44. Cahill, E.F., et al., *Hepatocyte Growth Factor Is Required for Mesenchymal Stromal Cell Protection Against Bleomycin-Induced Pulmonary Fibrosis.* Stem Cells Transl Med, 2016. **5**(10): p. 1307-1318.

45. Kennelly, H., B.P. Mahon, and K. English, *Human mesenchymal stromal cells exert HGF dependent cytoprotective effects in a human relevant pre-clinical model of COPD.* Sci Rep, 2016. **6**: p. 38207.

46. Cho, D.I., et al., *Antiinflammatory activity of ANGPTL4 facilitates macrophage polarization to induce cardiac repair.* JCI Insight, 2019. **4**(16).

47. Curley, G.F., et al., *Effects of intratracheal mesenchymal stromal cell therapy during recovery and resolution after ventilator-induced lung injury.* Anesthesiology, 2013. **118**(4): p. 924-32.

Figure Legends

Figure 1: PPARβ/δ(+) hBM-MSCs show enhanced reparative capacity of CALU-3 lung epithelial cells. (A) Experimental Design. A CALU-3 scratch assay was run, in combination with MSC-CM from PPARβ/**δ** agonized (+) or antagonized (-) hBM-MSCs. (B) Images of the wound healing assay at baseline or following 48hr were fixed and stained with crystal violet dye and (C) quantified using imageJ software (one-way ANOVA followed by Tukey's post-hoc test, n=3). (D) Using a mitomycin C proliferation inhibitor allowed for the investigation into the impact of this on migration or proliferation at different time-points (two-way ANOVA followed by Tukey's post-hoc test, n=3) and this was confirmed using (E) *TOP2A* gene expression by RT-PCR at a 48hr time-point (one-way ANOVA followed by Tukey's post-hoc test, n=3). Replicates are a representation of 3 individual hBM-MSC donors. Data is presented as mean ± SEM; *p<0.05, **p<0.01, ***p<0.001, ****p<0.0001.

Figure 2: PPARβ/δ(+) hBM-MSCs show enhanced expression of ANGPTL4 by RNA sequencing. (A) hBM-MSCs exposed to 1uM of PPARβ/**δ** agonist or antagonist were sent to Novogene™ for RNA sequencing. (B) Several DEGs were highlighted, and (C) the most significant hits were plotted on a volcano plot using Flourish™ software. Results were confirmed by assessing 2 known PPARβ/**δ** target genes in our sequencing dataset: (D) *ANGPTL4* and (E) *PDK4*. These results were confirmed by (F, G) RT-PCR (one-way ANOVA followed by Tukey's post-hoc test, n=3). Replicates are a representation of 3 individual hBM-MSC donors. Data is presented as mean ± SEM; *p<0.05, **p<0.01, ***p<0.001, ****p<0.0001.

Figure 3: PPARβ/δ(+) hBM-MSCs show enhanced expression of ANGPTL4, but not other traditional MSC-associated genes or proteins. Supernatant from hBM-MSCs exposed

to 1uM of PPARβ/**δ** agonist or antagonist were harvested before cells were collected in TRIzol for gene expression studies. Protein expression of (A) ANGPTL4, (B) VEGF and (C) MIF were assessed by ELISA and gene expression for (D) *PTGS2,* (E) *IL-6,* (F) *IDO,* (G) *PTGES* and (H) *TGFβ* were assessed (one-way ANOVA followed by Tukey's post-hoc test, n=3). Replicates are a representation of 3 individual hBM-MSC donors. Data is presented as mean ± SEM; *p<0.05, **p<0.01, ***p<0.001, ****p<0.0001.

Figure 4: PPARβ/δ(+) hBM-MSCs show enhanced wound repair via ANGPTL4. (A) Using an ANGPTL4 neutralisation approach, we assessed (B) wound closure of CALU-3 lung epithelial cells. (C) PPARβ/**δ**(+) hBM-MSCs showed enhanced wound closure, while ANGPTL4-neutralisation abrogated this effect. (D) Neutralisation of ANGPTL4 was confirmed by ELISA (one-way ANOVA followed by Tukey's post-hoc test, n=3). Replicates are a representation of 3 individual hBM-MSC donors. ND represents not-detected protein levels. Data is presented as mean ± SEM; *p<0.05, **p<0.01, ***p<0.001, ****p<0.0001.

Figure 5: ARDS patients have higher levels of PPARβ/δ(+) ligands and co-activators. (A) A publicly available dataset (Study ID: ST000042; doi: 10.21228/M8SG64) was mined for PPARβ/**δ** ligands present in the ARDS lung. (B) An additional dataset (GEO accession no.: GSE185263), based on ARDS serum, highlighted an increase in PPARβ/**δ**(+)-associated co-activators such as (C) *PPARGC1A*, (D) *NCOA1*, (E) *NCOA2*, (F) *NCOA3* and (G) *CREBBP;* and a decrease in PPARβ/**δ** (+)-associated co-repressors such as (H) *SIRT1*, (I) *NCOR1* and (J) *NCOR2* (one-way ANOVA followed by Tukey's post-hoc test, n=6+). Replicates are a representation of (A-J) individual ARDS patients, or healthy controls. (K) ANGPTL4 production from 3 individual hBM-MSC donors exposed to PPARβ/**δ** agonist (+) or antagonist

(-) in the presence or absence of 20% ARDS patient serum. Data is presented as mean ± SEM; *p<0.05, **p<0.01, ***p<0.001, ****p<0.0001.

Figure 6: ARDS-licensed MSC-CM$_{PPARβ/δ(+)}$ provides enhanced therapeutic effects in ALI in an ANGPTL4 dependent manner. Mice were exposed to 2mg/kg LPS IT, or PBS control. (A) An Evan's Blue Dye permeability assay was used to (B) quantify the amount of leakage from the lungs of mice exposed to LPS +/- our treatments of interest. Pro-inflammatory cytokines (C) TNFα and (D) IL-6 were assessed by ELISA and (E) total protein was assessed using a bradford assay (one-way ANOVA followed by Tukey's post-hoc test, n=3+). (F) Clinical scores and (G) % weigh loss were recorded over the course of the model. Replicates are a representation of individual mice. Data is presented as mean ± SEM; *p<0.05, **p<0.01, ***p<0.001, ****p<0.0001.

Graphical Abstract

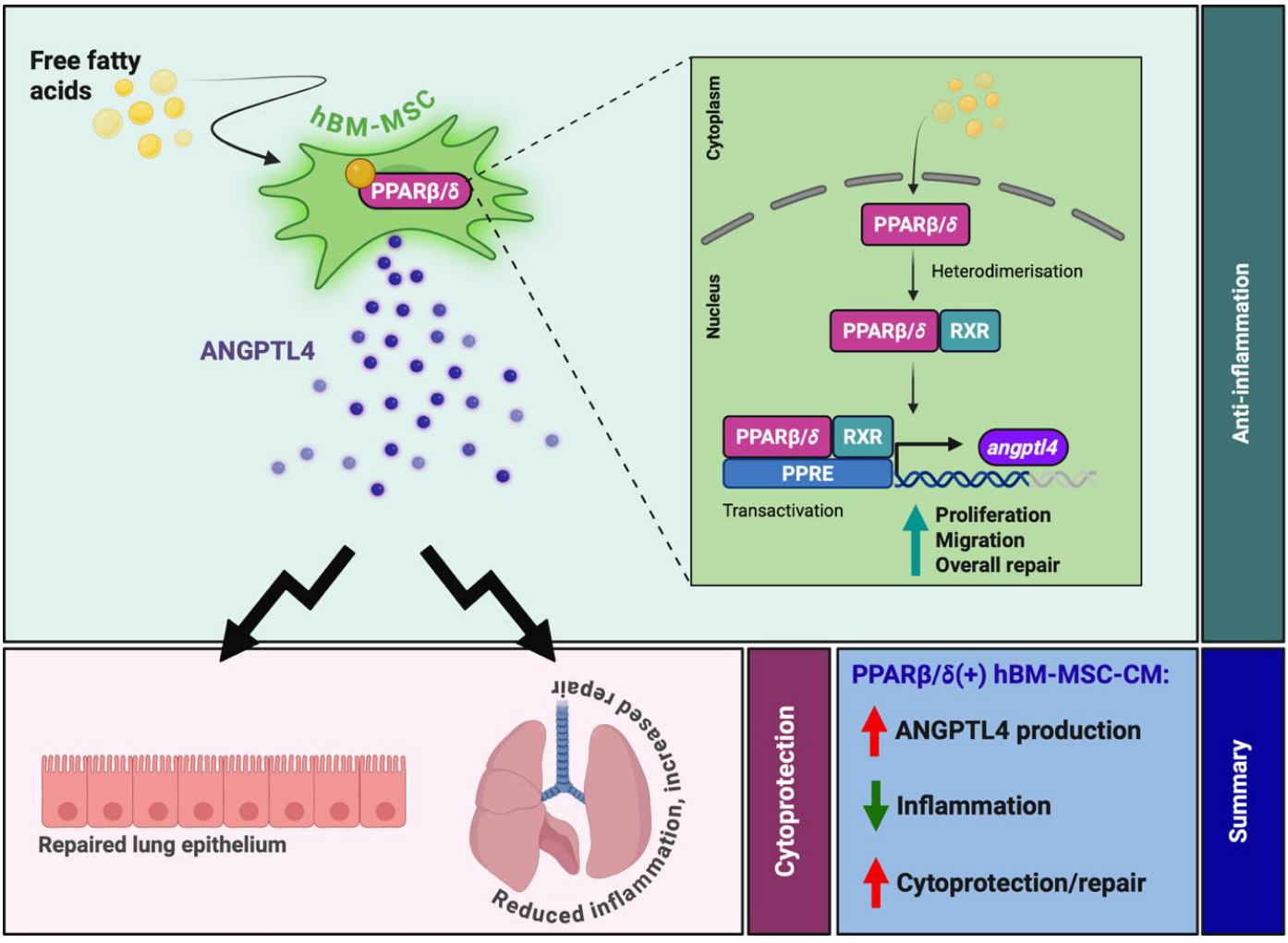

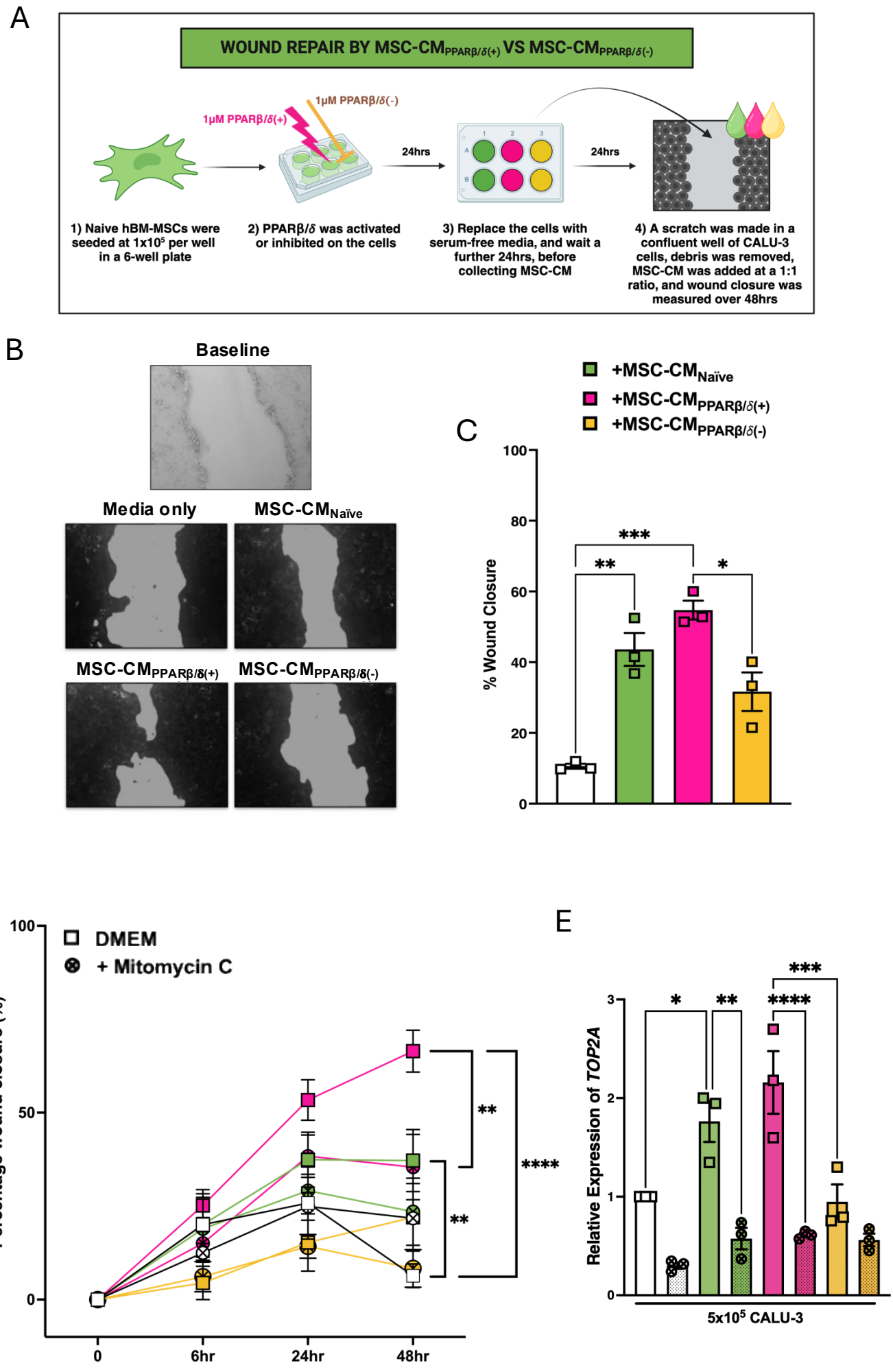
A
WOUND REPAIR BY MSC-CMPPARβ/δ(+) VS MSC-CMPPARβ/δ(-)
1μM PPARβ/δ(+)
1μM PPARβ/δ(-)
24hrs
24hrs
1) Naive hBM-MSCs were seeded at 1x10⁵ per well in a 6-well plate
2) PPARβ/δ was activated or inhibited on the cells
3) Replace the cells with serum-free media, and wait a further 24hrs, before collecting MSC-CM
4) A scratch was made in a confluent well of CALU-3 cells, debris was removed, MSC-CM was added at a 1:1 ratio, and wound closure was measured over 48hrs
B
Baseline
Media only
MSC-CMNaïve
MSC-CMPPARβ/δ(+)
MSC-CMPPARβ/δ(-)
C
+MSC-CMNaïve
+MSC-CMPPARβ/δ(+)
+MSC-CMPPARβ/δ(-)
% Wound Closure
100
80
60
40
20
0
***
**
*
D
DMEM
+ Mitomycin C
Percentage wound closure (%)
100
50
0
0
6hr
24hr
48hr
**
**
****
E
Relative Expression of TOP2A
3
2
1
0
*
**
****
***
5x10⁵ CALU-3

Figure 1

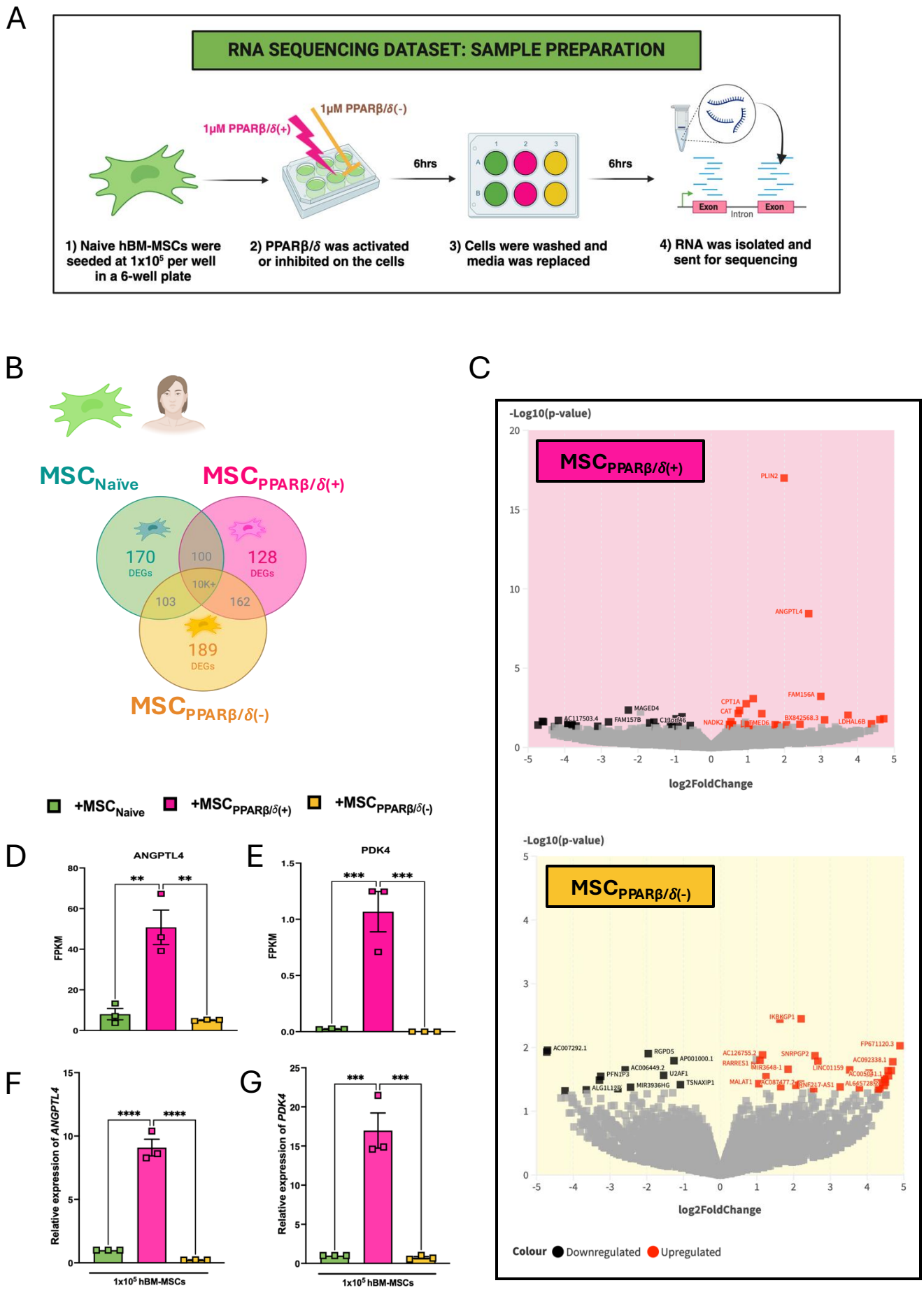
A
RNA SEQUENCING DATASET: SAMPLE PREPARATION
1μM PPARβ/δ(+)
1μM PPARβ/δ(-)
6hrs
6hrs
Exon
Intron
Exon
1) Naive hBM-MSCs were seeded at 1x10⁵ per well in a 6-well plate
2) PPARβ/δ was activated or inhibited on the cells
3) Cells were washed and media was replaced
4) RNA was isolated and sent for sequencing
B
MSCNaïve
MSCPPARβ/δ(+)
MSCPPARβ/δ(-)
170 DEGs
100
128 DEGs
10K+
103
162
189 DEGs
+MSCNaive
+MSCPPARβ/δ(+)
+MSCPPARβ/δ(-)
C
-Log10(p-value)
MSCPPARβ/δ(+)
PLIN2
ANGPTL4
FAM156A
log2FoldChange
-Log10(p-value)
MSCPPARβ/δ(-)
IKBKGP1
log2FoldChange
Colour Downregulated Upregulated
D
ANGPTL4
FPKM
E
PDK4
FPKM
F
Relative expression of ANGPTL4
1x10⁵ hBM-MSCs
G
Relative expression of PDK4
1x10⁵ hBM-MSCs

Figure 2

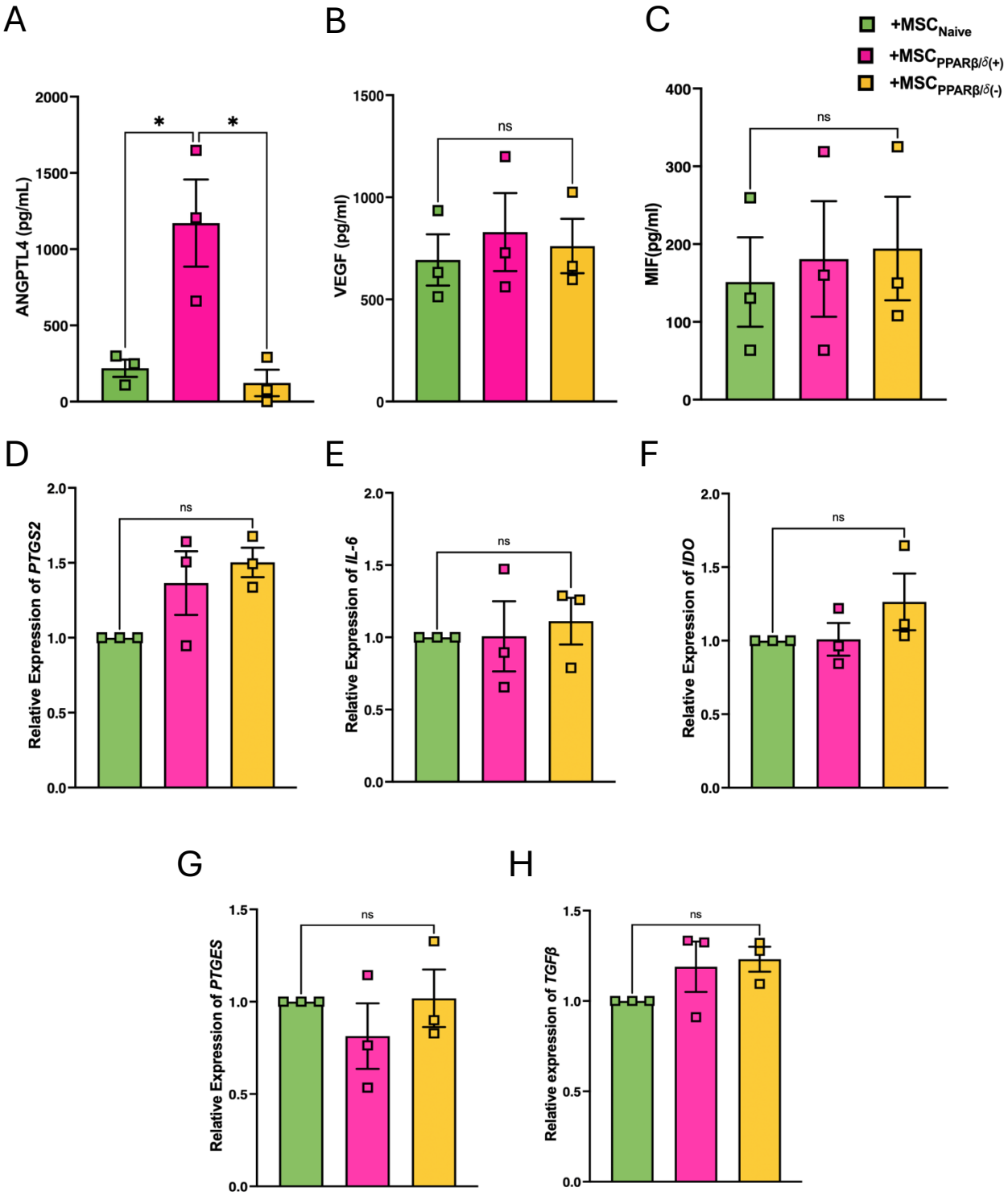
A
B
C
+MSC$_{Naive}$
+MSC$_{PPARβ/δ(+)}$
+MSC$_{PPARβ/δ(-)}$
ANGPTL4 (pg/mL)
VEGF (pg/ml)
MIF(pg/ml)
ns
D
E
F
Relative Expression of PTGS2
Relative Expression of IL-6
Relative Expression of IDO
G
H
Relative Expression of PTGES
Relative expression of TGFβ

Figure 3

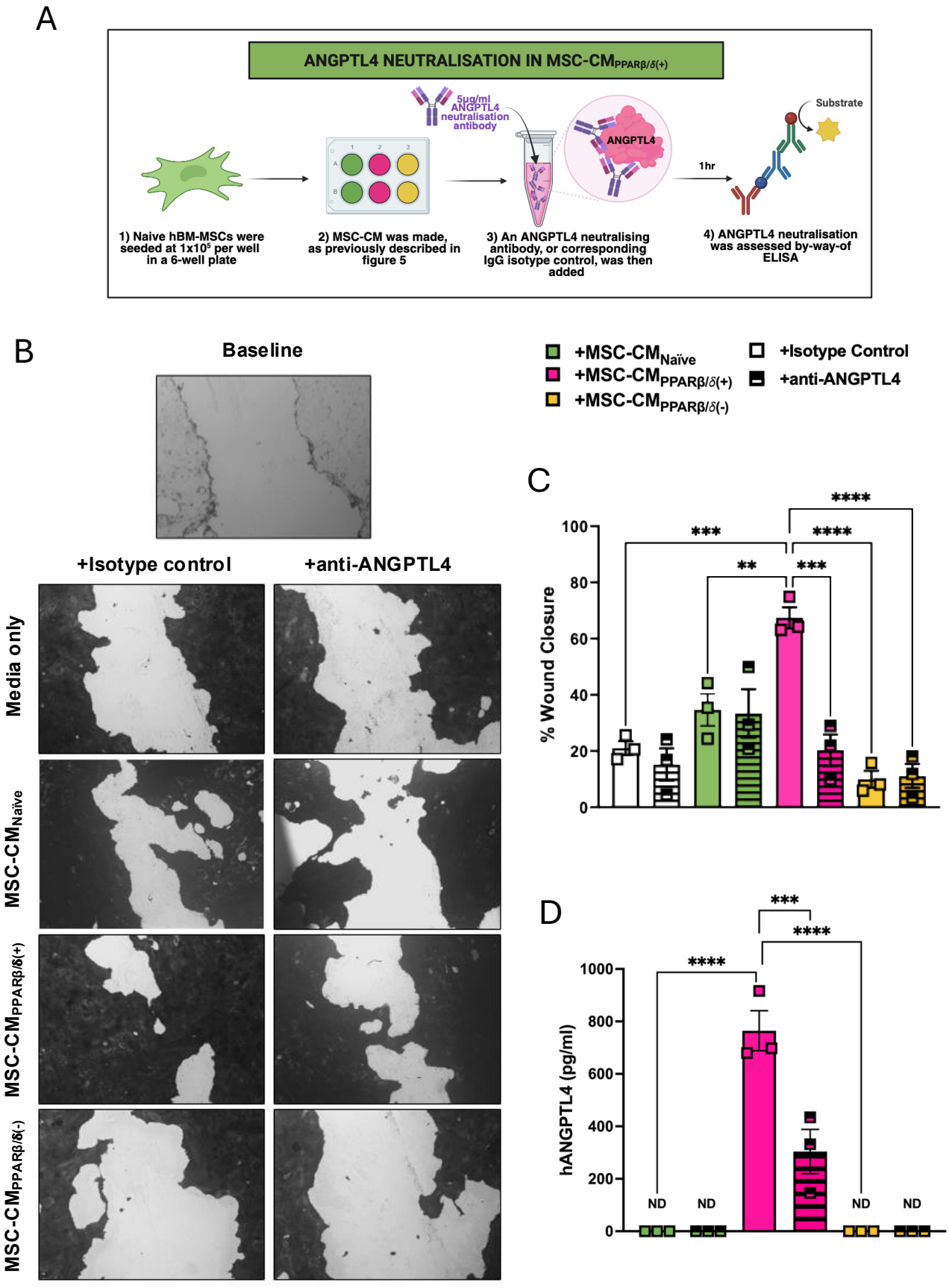
A
ANGPTL4 NEUTRALISATION IN MSC-CMPPARβ/δ(+)
5µg/ml ANGPTL4 neutralisation antibody
ANGPTL4
Substrate
1hr
1) Naive hBM-MSCs were seeded at 1x10⁵ per well in a 6-well plate
2) MSC-CM was made, as previously described in figure 5
3) An ANGPTL4 neutralising antibody, or corresponding IgG isotype control, was then added
4) ANGPTL4 neutralisation was assessed by-way-of ELISA
B
Baseline
+Isotype control
+anti-ANGPTL4
Media only
MSC-CMNaïve
MSC-CMPPARβ/δ(+)
MSC-CMPPARβ/δ(-)
+MSC-CMNaïve
+MSC-CMPPARβ/δ(+)
+MSC-CMPPARβ/δ(-)
+Isotype Control
+anti-ANGPTL4
C
% Wound Closure
100
80
60
40
20
0
***
****
**
***
****
D
hANGPTL4 (pg/ml)
1000
800
600
400
200
0
***
****
****
ND
ND
ND
ND

Figure 4

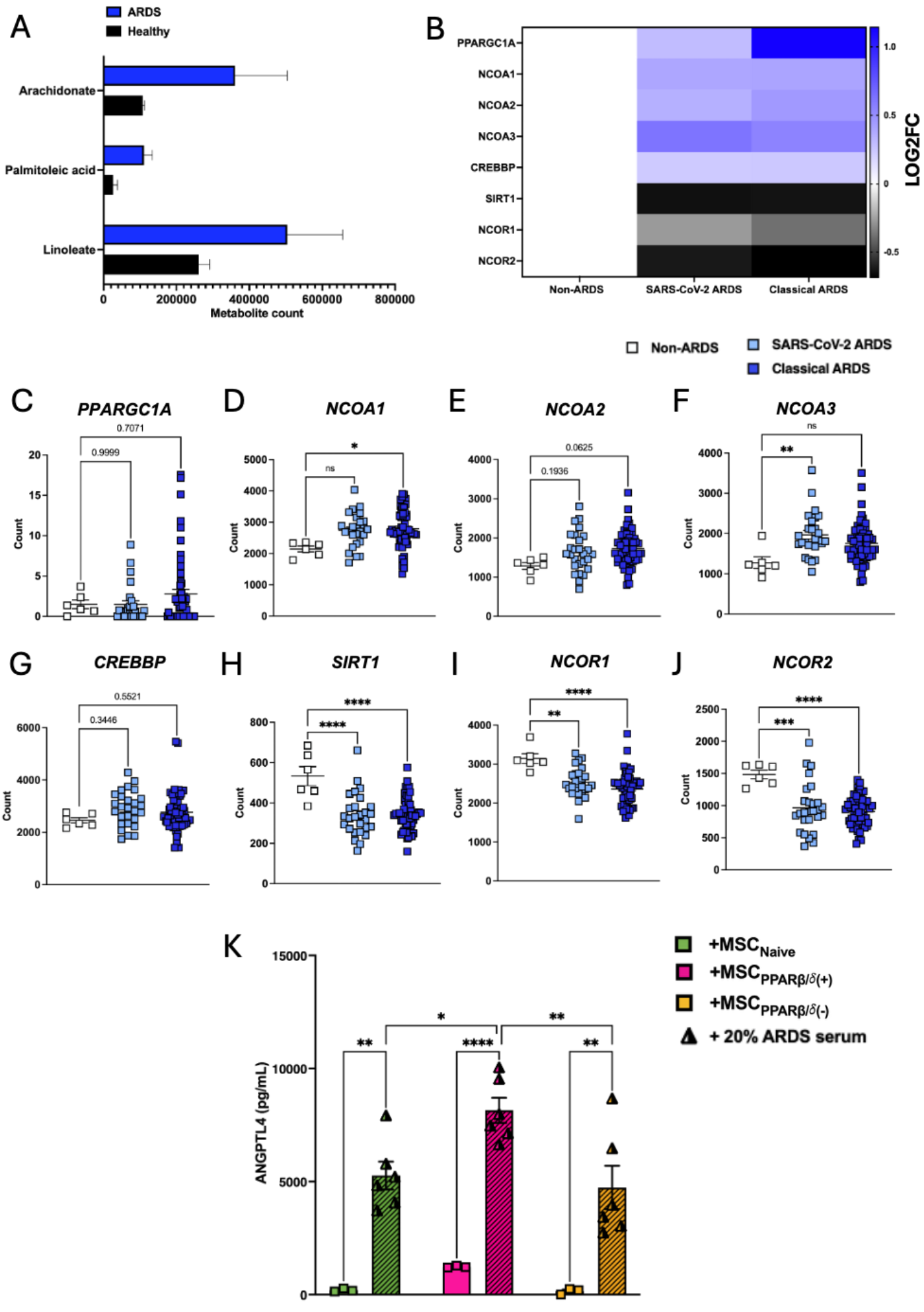
A
ARDS
Healthy
Arachidonate
Palmitoleic acid
Linoleate
0
200000
400000
600000
800000
Metabolite count
B
PPARGC1A
NCOA1
NCOA2
NCOA3
CREBBP
SIRT1
NCOR1
NCOR2
Non-ARDS
SARS-CoV-2 ARDS
Classical ARDS
LOG2FC
1.0
0.5
0
-0.5
Non-ARDS
SARS-CoV-2 ARDS
Classical ARDS
C
PPARGC1A
0.7071
0.9999
Count
D
NCOA1
ns
*
E
NCOA2
0.0625
0.1936
F
NCOA3
ns
**
G
CREBBP
0.5521
0.3446
H
SIRT1
****
****
I
NCOR1
****
**
J
NCOR2
****
***
K
ANGPTL4 (pg/mL)
15000
10000
5000
0
*
**
**
****
**
+MSC$_{Naive}$
+MSC$_{PPARβ/δ(+)}$
+MSC$_{PPARβ/δ(-)}$
+ 20% ARDS serum

Figure 5

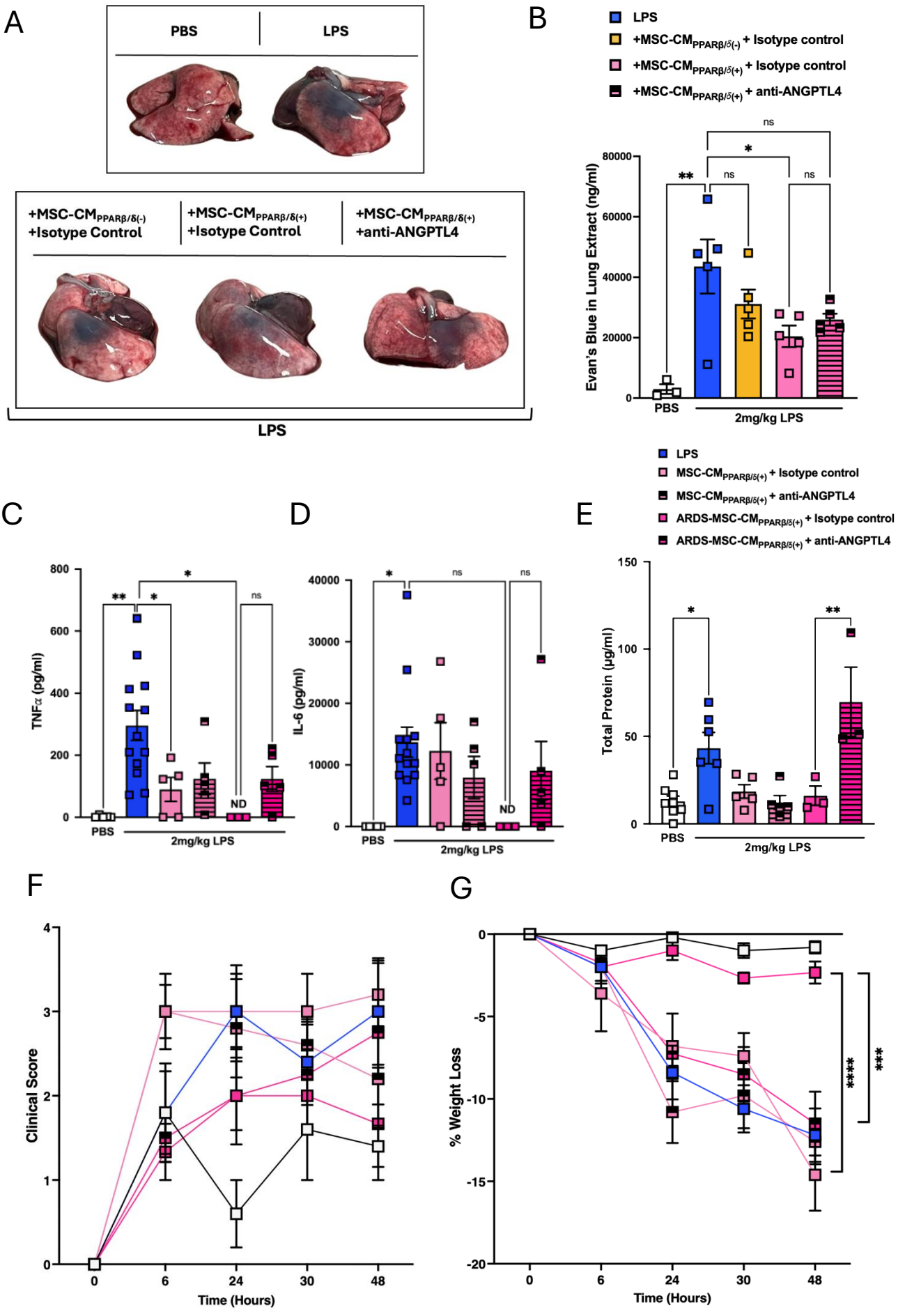
A
PBS
LPS
+MSC-CM$_{PPARβ/δ(-)}$ +Isotype Control
+MSC-CM$_{PPARβ/δ(+)}$ +Isotype Control
+MSC-CM$_{PPARβ/δ(+)}$ +anti-ANGPTL4
LPS
B
LPS
+MSC-CM$_{PPARβ/δ(-)}$ + Isotype control
+MSC-CM$_{PPARβ/δ(+)}$ + Isotype control
+MSC-CM$_{PPARβ/δ(+)}$ + anti-ANGPTL4
Evan's Blue in Lung Extract (ng/ml)
PBS
2mg/kg LPS
C
TNFα (pg/ml)
ND
D
IL-6 (pg/ml)
E
LPS
MSC-CM$_{PPARβ/δ(+)}$ + Isotype control
MSC-CM$_{PPARβ/δ(+)}$ + anti-ANGPTL4
ARDS-MSC-CM$_{PPARβ/δ(+)}$ + Isotype control
ARDS-MSC-CM$_{PPARβ/δ(+)}$ + anti-ANGPTL4
Total Protein (μg/ml)
F
Clinical Score
Time (Hours)
G
% Weight Loss
Time (Hours)

Figure 6